ARTICLE

High-quality EuO thin films the easy way via topotactic transformation

Thomas Mairoser[1], Julia A. Mundy[2], Alexander Melville[3], Daniel Hodash[3], Paul Cueva[2], Rainer Held[3], Artur Glavic[4], Jürgen Schubert[5], David A. Muller[2,6], Darrell G. Schlom[3,6] & Andreas Schmehl[1]

Epitaxy is widely employed to create highly oriented crystalline films. A less appreciated, but nonetheless powerful means of creating such films is via topotactic transformation, in which a chemical reaction transforms a single crystal of one phase into a single crystal of a different phase, which inherits its orientation from the original crystal. Topotactic reactions may be applied to epitactic films to substitute, add or remove ions to yield epitactic films of different phases. Here we exploit a topotactic reduction reaction to provide a non-ultra-high vacuum (UHV) means of growing highly oriented single crystalline thin films of the easily over-oxidized half-metallic semiconductor europium monoxide (EuO) with a perfection rivalling that of the best films of the same material grown by molecular-beam epitaxy or UHV pulsed-laser deposition. As the technique only requires high-vacuum deposition equipment, it has the potential to drastically improve the accessibility of high-quality single crystalline films of EuO as well as other difficult-to-synthesize compounds.

[1] Zentrum für Elektronische Korrelationen und Magnetismus, Universität Augsburg, Universitätsstraße 1, 86159 Augsburg, Germany. [2] School of Applied and Engineering Physics, Cornell University, Ithaca, New York 14853, USA. [3] Department of Materials Science and Engineering, Cornell University, Ithaca, New York 14853, USA. [4] Quantum Condensed Matter Division, Oak Ridge National Laboratory, Oak Ridge, Tennessee 37831, USA. [5] Peter Grünberg Institute, PGI 9-IT, JARA-FIT, Research Centre Jülich, 52425 Jülich, Germany. [6] Kavli Institute at Cornell for Nanoscale Science, Ithaca, New York 14853, USA. Correspondence and requests for materials should be addressed to D.G.S. (email: schlom@cornell.edu).

1

Europium metal can adopt three stable valence states, Eu^{2+} in europium monoxide (EuO, rock salt structure, space group $Fm\bar{3}m$) (ref. 1), $Eu^{2\,2/3+}$ in Eu_3O_4 (orthorhombic structure, space group $Pnma$)[2] and Eu^{3+} in Eu_2O_3 (monoclinic or cubic structure, space groups $C2/m$ or $Ia\bar{3}$, respectively)[3,4]. Of these phases, EuO is scientifically the most interesting compound, mainly because it is a rare example of a high-magnetization ferromagnetic semiconductor ($7\,\mu_B$ per Eu; $T_C = 69\,K$) (ref. 5) which can be epitactically integrated with silicon[6], GaAs[7], GaN[6], graphene[8], diamond[9] and many oxide substrates. It is a half metal with over 96% spin polarization and can be conductance matched to silicon by rare-earth doping, rendering it an ideal candidate for spintronic applications[6,10]. In addition, it shows a plethora of giant transport and magneto-optic properties, which makes it a fascinating material for basic research as well as device applications[6].

As EuO has its highest potential when epitactically integrated with spintronic-relevant semiconductors, the requirements with respect to the structural perfection of EuO films are basically the same as for all other semiconductor applications. Decades of technological innovation make it possible to fabricate silicon and other mainstream semiconductors with unrivalled perfection. For thin films, the standard methods all involve epitaxy—utilizing liquids (liquid-phase epitaxy), gases (vapour-phase epitaxy) or solids (solid-phase epitaxy). In this process, the atoms in the film inherit their crystalline arrangement from the underlying single crystal on which they are deposited and with which they do not react. If the depositing materials react with the substrate, the result is often disastrous to the crystalline perfection of the product formed, but an exception exists: topotaxy. Here the product inherits its highly oriented structure from the single crystal it replaced[11].

Although rare, topotactic transformations can occur as materials oxidize (for example, Fe to FeO, Cu to Cu_2O) (ref. 12), alter their hydrogen content (for example, FeO(OH) to Fe_2O_3) (ref. 11), swap anions (for example, ZnS to ZnO) (ref. 13) or undergo phase transitions[14] (for example, the α to β transition in quartz)[11]. They are known for many mineral systems (for example, the formation of spinel from sapphire and periclase)[11,15] and have even been observed in meteorites[16]. Most involve the substitution or addition of ions to a structure, but examples involving reduction are known[17–22] and have been used to create epitactic films of phases that are otherwise inaccessible including $LaNiO_2$, $SrFeO_2$, $CaFeO_2$ and even superlattices of these topotactically transformed phases[23–26]. This approach is being exploited in thin films due to its experimental simplicity[27], for example, the formation of $SrFeO_{3-\varsigma}F_{\gamma}$ from epitactic $SrFeO_{3-x}$ films, where the corrosive fluorine can be introduced ex situ after the epitactic film growth is complete[28].

In many metal oxides the desired physical properties depend strongly on the structure of the compound, which often can be delicately controlled by altering the oxygen stoichiometry and thereby the oxidation state or valence of the involved metals. Controlling the oxygen stoichiometry is therefore of great importance in the preparation of oxides in the form of epitactic thin films for basic research or applications. For many materials, the desired phase is the fully oxidized one and its synthesis merely requires a sufficiently oxidizing environment during deposition. This makes their growth comparatively easy, for example, by reactive sputtering, molecular-beam epitaxy (MBE) or pulsed-laser deposition (PLD) in a (relatively) high-pressure ambient of oxygen or even ozone. For the case of EuO, however, the phase with the lowest oxidation state shows by far the most interesting physical properties. To access this phase one faces much higher demands, mainly the need to provide a controlled environment that is neither too oxidative nor too reducing during both growth and cooling following growth.

In this Article we demonstrate an alternative approach that does not require ultra-high-vacuum (UHV) equipment to grow high-quality EuO films, but can be executed in standard high-vacuum deposition systems, which are much more abundant. This technique allows the growth of single crystalline EuO films by magnetron sputtering under high-vacuum conditions with crystalline quality surpassing that of the best films grown by UHV techniques. The growth mechanism is based on a chemical reduction of an epitactic Eu_2O_3 precursor film into single crystalline EuO by chemical reduction. As the resulting high-quality EuO film inherits its crystalline structure form the precursor film, the reduction reaction is a topotactic transformation.

Results

Stability requirements and growth kinetics. At room temperature Eu^{2+} is only thermodynamically stable in minuscule oxygen partial pressures (below 10^{-64} atm)[29], making its growth as well as subsequent ex situ processing highly demanding[6]. This instability in ambient conditions has, up to now, limited the growth of epitactic EuO films with high crystalline quality to UHV MBE[6–10,30,31] and UHV PLD[32,33]. Sputtering of EuO films from an EuO target[34,35] or multiple targets (Eu metal and Eu_2O_3) (refs 36,37) has been reported, but resulted in polycrystalline, multiphase films, even when grown in a UHV deposition system.

For multivalent metals, thermodynamically relevant pressure values can be derived from Ellingham diagrams. According to thermodynamics, at 700 K, europium will only be stable in its lowest oxidation state (Eu^{2+} in EuO) if the oxygen partial pressure lies between 5×10^{-80} and 2×10^{-57} atm[29,38]. For thin-film growth, the kinetics of oxidation are also important[39–41]. To form EuO from incident molecular beams of europium and oxygen, the partial pressure of oxygen must be precisely calibrated so that the ratio of the sticking coefficients of europium atoms and O_2 molecules imping on the film surface per unit time is 2:1. Deviations from this ratio lead to defects such as oxygen vacancies or higher Eu-oxides such as Eu_3O_4 and Eu_2O_3, unless self-limiting processes can be utilized. Because of this difficulty, EuO thin films are typically grown with adsorption-controlled techniques[30] requiring well-controlled oxygen partial pressures in the UHV range and limiting deposition temperatures to values above $\sim 400\,°C$. Also, epitactic growth of many other multivalent metals requires sophisticated and expensive deposition equipment such as UHV MBE or PLD systems effectively limiting the access to high-quality epitactic films of such materials.

Four-circle X-ray diffraction (XRD) structural analysis. The crystalline quality of all films was investigated using four-circle XRD. To demonstrate the transformation reaction, two Eu_2O_3 films were deposited simultaneously on (110) $YAlO_3$ (ref. 42). Sample 1 was then taken out of the sputter system, while (after air exposure) sample 2 was heated back up to $T_D \approx 580\,°C$ and capped with titanium as described in Methods. Figure 1a shows the θ–2θ-scans of both samples. Sample 1 corresponds to (401)-oriented single-phase monoclinic Eu_2O_3. The θ–2θ-scan of sample 2, however, corresponds to a (001)-oriented single-phase EuO film. The orientation relationships between the films and substrates were determined by off-axis XRD scans. Figure 1b shows ϕ-scans of the $YAlO_3$ substrate and the Eu_2O_3 film of sample 1. In combination with calculated orientation relationships (Supplementary Figs 1 and 2 and Supplementary Table 1), the data shows epitactic growth with an in-plane orientation relationship $[0\bar{1}0]_{Eu_2O_3} \parallel [001]_{YAlO_3}$. The ϕ-scans of sample 2 (Fig. 1c) correspond to single crystalline EuO with an in-plane orientation relationship to the substrate of $[1\bar{1}0]_{EuO} \parallel [001]_{YAlO_3}$. Rocking curves of the Eu_2O_3 401 peak and the EuO 002 peak
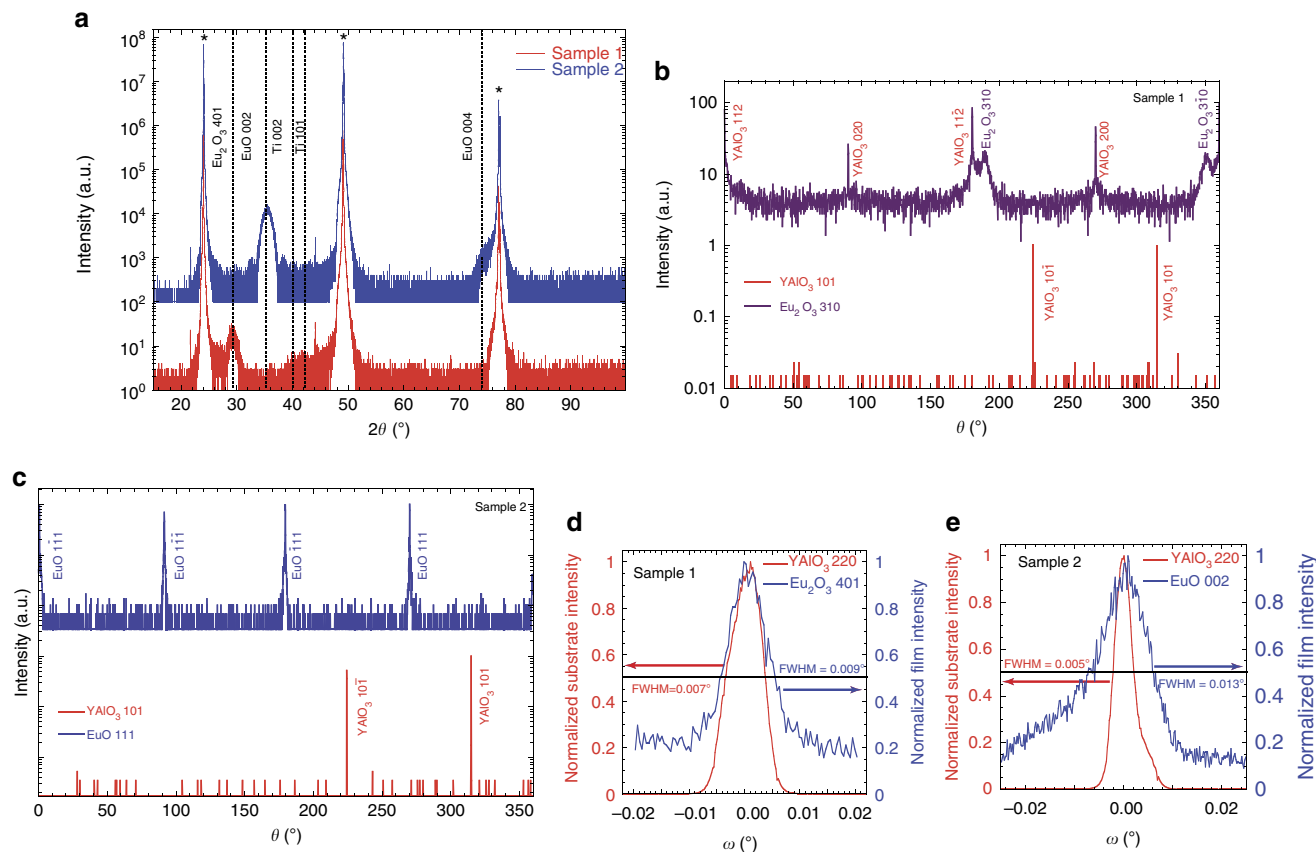
Figure 1 | Establishing the orientation relationship of the topotactic transformation. (a) θ–2θ-scans of a single-phase (401)-oriented Eu_2O_3 film (sample 1) and a single-phase (001)-oriented EuO film capped with titanium (sample 2) grown on (110) $YAlO_3$. Thickness fringes are present around the EuO 002 peak. Substrate peaks are marked by asterisks. **(b)** ϕ-scans of the $YAlO_3$ 101 and the monoclinic Eu_2O_3 310 families of peaks. These scans demonstrate the epitactic growth of the Eu_2O_3 film with in-plane orientation relationship $[0\bar{1}0]_{Eu_2O_3} \parallel [001]_{YAlO_3}$ (scan parameters: $2\theta_{Eu_2O_3} = 31.60°$; $\psi_{Eu_2O_3} = 49.84°$; $2\theta_{YAlO_3} = 21.05°$; $\psi_{YAlO_3} = 53.40°$). **(c)** ϕ-scans of the $YAlO_3$ 101 and the EuO 111 families of peaks. The four EuO peaks demonstrate the topotactic conversion of Eu_2O_3 into an untwinned (001)-oriented EuO film on the (110) $YAlO_3$ substrate with in-plane orientation relationships $[1\bar{1}0]_{EuO} \parallel [001]_{YAlO_3}$ (scan parameters: $2\theta_{EuO} = 30.08°$; $\psi_{EuO} = 52.50°$; $2\theta_{YAlO_3} = 21.03°$; $\psi_{YAlO_3} = 53.42°$). **(d)** Rocking curves of the $YAlO_3$ 220 peak and the Eu_2O_3 401 peak, measured on sample 1, respectively. The FWHM of the film peak is comparable to that of the substrate peak, indicating the excellent crystalline quality. **(e)** Rocking curves of the $YAlO_3$ 220 peak and the EuO 002 peak, measured on sample 2, respectively. The FWHM of the film peak is only slightly larger than that of the film peak of sample 1.

(Fig. 1d,e) demonstrate the outstanding crystalline quality of the Eu_2O_3 and the EuO films, respectively. The full width at half maximum (FWHM) of the Eu_2O_3 401 peak of 0.009° is comparable to that of the substrate (0.007°). The FWHM of 0.013° of the EuO 002 peak of sample 2 is only slightly larger (Fig. 1e). For samples where the titanium layer was deposited *in situ*, directly after the Eu_2O_3 deposition, a FWHM of the EuO 002 peak as small as 0.004° has been observed using a substrate with a comparably small FWHM. This is the smallest value reported in the literature, smaller even than the best films grown by MBE or UHV PLD[30,33]. Using X-ray reflectometry, a root-mean-squared (r.m.s.) interface roughness of 0.28 nm between the EuO film and the TiO_x layer was measured. This value is smaller than the r.m.s. roughness of the substrate surface measured by X-ray reflectometry of 0.70 nm, indicating a high-quality interface (Supplementary Fig. 4).

As the XRD data demonstrate, it is the hot capping of the Eu_2O_3 with titanium that leads to a reduction of the precursor films to single crystalline, topotactic, high-quality EuO films. During this reaction the titanium metal is oxidized to TiO_x. This reduction induced by the titanium capping is a topotactic transformation, a chemical reaction that results in a material with a crystalline orientation related to the starting product[11,43,44].

STEM and EELS analysis. To verify this transformation mechanism and to characterize the film microstructure, europium valence and interface abruptness, the same samples shown in Fig. 1 were investigated by scanning transmission electron microscopy (STEM) and electron energy-loss spectroscopy (EELS). Figure 2a shows the high-angle annular dark field (HAADF) signal from the Eu_2O_3 film (sample 1) and Fig. 2b shows the HAADF signal from the EuO film (sample 2). The Eu_2O_3 film is epitactic to the substrate and exhibits distinct Eu^{3+} valence revealed by EELS. The Eu^{2+} and Eu^{3+} Eu–$N_{4,5}$ edges are shown in Fig. 2c[45,46]. The transformed EuO film, sample 2, also formed a coherent interface with the $YAlO_3$ substrate. A diffractogram from the film (Fig. 1a) shows a pattern consistent with the EuO rock salt crystal structure. The EELS signal depicted in Fig. 2c shows a distinct fingerprint, consistent with the Eu^{2+} state[45,46]. Lateral scans across the film did not yield any variations in the europium valence as would be expected for a film with predominately EuO and potentially small remnant inclusions of Eu_2O_3 (or Eu_3O_4). Therefore, we conclude that the film is phase pure and does not contain any remnant inclusions of Eu_2O_3 or Eu_3O_4 within the detection limit of EELS.

The transformation of the Eu_2O_3 precursor film to EuO is driven by chemical reduction with titanium being the reducing

agent. The reduction of Eu^{3+} to Eu^{2+} is described by the chemical reaction: $Eu_2O_3 + Ti \rightarrow 2\,EuO + TiO$ with $\Delta G°$ of -461 and $-423\,kJ\,mol^{-1}$ at 300 and 900 K, respectively[29,38]. The formation of the monoxide of titanium (TiO) is energetically favoured (Supplementary Table 2). From these free energies of reaction and the ideal gas constant R, the equilibrium constant

$$\ln K = -\frac{\Delta G°}{RT} \qquad (1)$$

of this reaction can be calculated to be $K_{300\,K} = 5.9 \times 10^{80}$ and $K_{900\,K} = 1.6 \times 10^{74}$. The equilibrium constant is much larger than one, indicating the almost complete conversion of Eu^{3+} into Eu^{2+}. Note that the formation of europium metal is thermodynamically disallowed because of the positive value of $\Delta G°$ for all corresponding formation reactions (Supplementary Table 2). Presumably the same reason precludes the formation of Eu_3O_4, though we are not aware of free energy data for Eu_3O_4.

As the reduction of Eu^{3+} to Eu^{2+} requires oxygen diffusion from the precursor film to the titanium capping layer, the transformation propagates from the titanium layer into the Eu_2O_3 film. Figure 2d shows a HAADF-STEM image and Fig. 2e, the valence analysis of the EELS signal of an only partially reduced film. The EELS signal was fitted with a linear least square optimization to the europium reference spectra shown in Fig. 2c to determine the spatial variance in the europium valence. Close to the titanium layer, only Eu^{2+} is present, whereas near the substrate, only Eu^{3+} can be found. The depth of the reduction strongly depends on the oxygen diffusion length and hence on the substrate
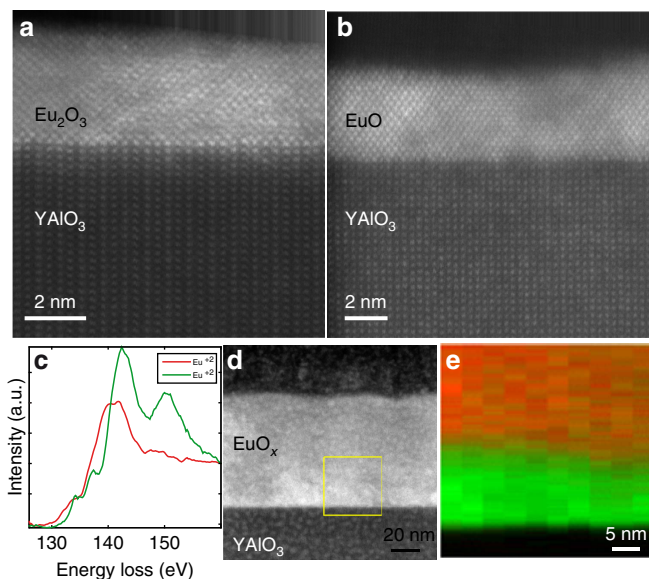
temperature during the titanium deposition. We find that at room temperature <1 nm of the Eu_2O_3 is reduced to EuO, whereas at 600 °C at least 60 nm of EuO can be transformed. We note that the partially oxidized titanium capping layer protects the EuO film from re-oxidation when exposed to air. This allows *ex situ* measurements of the films without the need for further protection.

Magnetic properties. The high crystalline quality results in excellent physical properties of the transformed EuO films. The Curie temperature (T_C) and the magnetic field dependence of the magnetization ($M(T)$ and $M(\mu_0H)$) of the films were determined using superconducting quantum interference device magneto-metry. Figure 3a shows a typical zero-field $M(T)$ measurement from which $T_C = 70 \pm 1$ K was determined[47]. This value equals that of bulk EuO (ref. 48). Figure 3b shows the in-plane $M(\mu_0H)$ characteristic at $T = 5$ K of the same film. The saturation magnetization of $6.4^{+0.8}_{-0.5}\,\mu_B$ per Eu is in good agreement with the expected saturation magnetization of $7\,\mu_B$ per Eu originating from the $4f$ (ref. 7) electronic configuration of Eu^{2+} (ref. 5). The very low coercive field of 50 ± 10 G is again consistent with the excellent crystalline quality of the film.

Discussion

From the orientation relationship between the initial epitactic Eu_2O_3 film and the (110) $YAlO_3$ substrate on which it was grown

Figure 2 | Characterization of the europium valence and film microstructure. (**a**) Cross-sectional HAADF-STEM image of the Eu_2O_3 film (sample 1). (**b**) Cross-sectional HAADF-STEM image of the transformed EuO film (sample 2) viewed along the [110] zone axis of the EuO film and the [$\bar{1}$10] zone axis of the $YAlO_3$. See Supplementary Fig. 3 for a lower magnification STEM image of this same sample showing a larger area. (**c**) EELS fine structure analysis of the EuO $M_{4,5}$ edge. Distinct EELS fingerprints corresponding to the occurrence of only Eu^{3+} in sample 1 and of only Eu^{2+} in sample 2, respectively. (**d**) Cross-sectional HAADF-STEM image of a partially reduced EuO film. The EELS analysis was performed on the region indicated by the yellow box. A non-negative nonlinear least squares fit to the components in **c** reveals the distribution of the EuO (Eu^{2+} is shown in red) and Eu_2O_3 (Eu^{3+} is shown in green) in the partially reduced film as shown in (**e**). Streaks at the top of the STEM images are an artifact of post-acquisition drift correction.
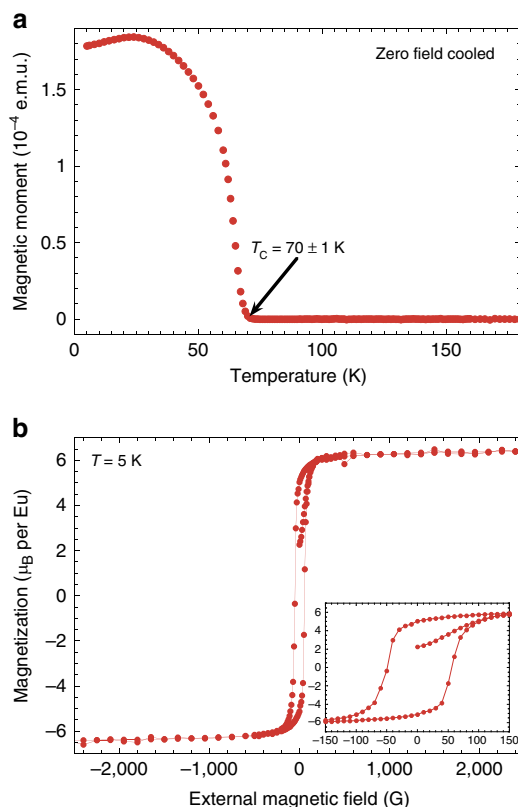
Figure 3 | Magnetic properties of topotactic EuO. (**a**) Spontaneous magnetization $M(T)$ of an EuO film grown on (110) $YAlO_3$ via a topotactic transformation, measured using superconducting quantum interference device magnetometry in zero external field. Both the shape of the $M(T)$ curve and the extracted T_C is typical of EuO films. The decrease of $M(T)$ at low temperatures is due to domain effects. (**b**) $M(\mu_0H)$ curve of the same sample. The saturation magnetization of the film was determined to be $6.4^{+0.8}_{-0.5}\,\mu_B$ per Eu. The inset shows a magnified view of the hysteresis curve, which has a coercive field of 50 ± 10 G.

(Supplementary Fig. 1) and the orientation relationship of the topotactically transformed EuO film with this same substrate (Supplementary Fig. 2), we know the alignment between the reactant and product phases: $(401)_{Eu_2O_3} \parallel (001)_{EuO}$ with $[0\bar{1}0]_{Eu_2O_3} \parallel [1\bar{1}0]_{EuO}$. This orientation relationship is shown in Fig. 4. Motifs of structural similarity and a reasonable lattice match (-1.0% along $[0\bar{1}0]_{Eu_2O_3} \parallel [1\bar{1}0]_{EuO}$ and -5.8% along $[\bar{1}04]_{Eu_2O_3} \parallel [\bar{1}10]_{EuO}$) are evident between the (401) Eu_2O_3 and (001) EuO planes. Interestingly, the shortest distance between europium atoms in the Eu_2O_3 before the topotactic transformation

(the $[\bar{1}04]_{Eu_2O_3}$ direction) ends up being nearly parallel to the shortest distance between europium atoms in the EuO following the transformation (the $[\bar{1}10]_{EuO}$ direction). This same behaviour has also been noted in other topotactic transformations: Fe to FeO (ref. 49) and Ba to BaO (ref. 50). A plausible pathway for the topotactic transformation between Eu_2O_3 and EuO is shown in Fig. 4. The closely packed (401) plane of Eu_2O_3 in Fig. 4b,c has composition EuO. Shifting the indicated columns of atoms in the (401) plane of Eu_2O_3 by 1.8 Å along $[0\bar{1}0]_{Eu_2O_3}$ (see Fig. 4c) results in virtually identical atomic patterns in the (401) Eu_2O_3 and (001) EuO planes.
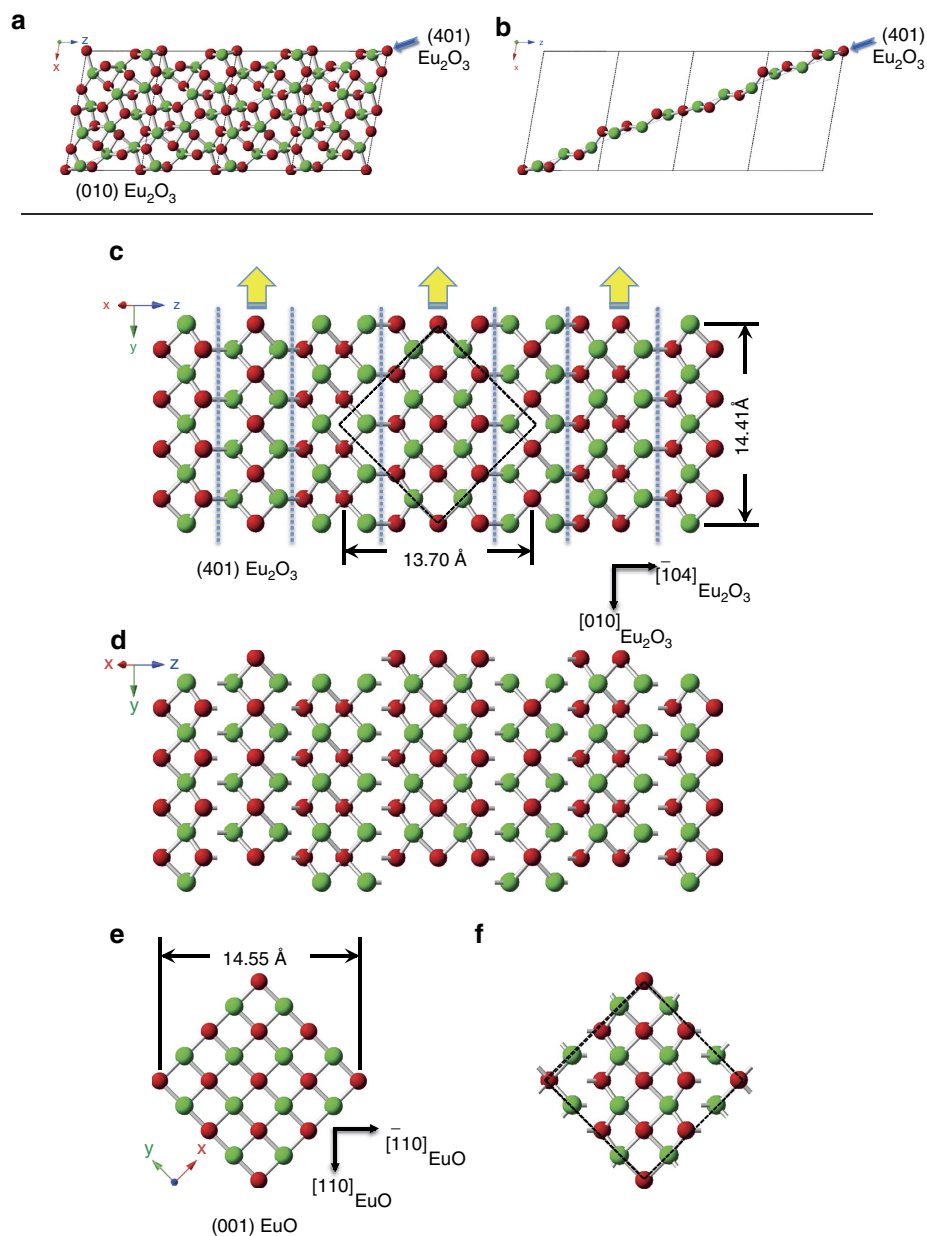
Figure 4 | A comparison of the atomic arrangements of the (401) Eu₂O₃ and (001) EuO planes. (**a**) The crystal structure of the monoclinic polymorph of Eu_2O_3 viewed along the [010] zone axis. The unit cell of Eu_2O_3 is outlined with dashed lines and the (401) plane, which is viewed edge-on, is indicated by the blue line. (**b**) The atoms closest to the chosen (401) plane (the blue line) have overall composition EuO and form a closely packed layer. (**c**) The (401) plane of atoms selected in **b** viewed at normal incidence. The atomic arrangement is similar to that of the (001) EuO plane and can be made virtually identical by shifting the columns of atoms between the dashed lines in the direction of the yellow arrows by $\frac{b}{2}[0\bar{1}0]$. (**d**) The (401) plane of Eu_2O_3 after performing the atomic shifts described in **c**. (**e**) The (001) EuO plane. (**f**) Emphasizes the similarity in atomic arrangement between **d** and **e**, by showing the overlap unit cell of shifted $(401)_{Eu_2O_3}$. The overlap unit cell between $(401)_{Eu_2O_3}$ and $(001)_{EuO}$ is also shown by the dashed quadrilateral (a rhombus for $(401)_{Eu_2O_3}$ and a square for $(001)_{EuO}$) in **c**, before any shift of the atomic positions.

In conclusion, we have demonstrated the topotactic transformation of epitactic Eu_2O_3 films grown on (110) $YAlO_3$ into high-quality, single crystalline EuO films by a titanium-induced chemical reduction. The approach only requires high-vacuum deposition equipment, overcoming the prior need for UHV deposition systems to grow films of comparable quality. STEM, EELS and superconducting quantum interference device measurements corroborate the growth mechanism and the excellent quality of the transformed EuO films. The method used is general; provided the structures of the precursor and the target films are closely related, the transformations are expected to be topotactic leading to high-quality single crystalline films.

Methods

Film growth. All films were grown in a high-vacuum sputter deposition system (base pressure $\approx 3 \times 10^{-7}$ mbar) using 3″ targets (99.99% purity). In the course of this study, the sputtering system was equipped with a more powerful vacuum pump, reducing the base pressure to $\approx 3 \times 10^{-8}$ mbar with no detectable changes in film quality. The films were grown on single crystalline $YAlO_3$ substrates oriented within 0.2° of (110). (110) oriented $YAlO_3$ provides a rectangular surface net with in-plane lattice constants 7.431 Å along $[\bar{1}10]$ and 7.370 Å along [001] at room temperature[42]. EuO is cubic with lattice constant 5.144 Å at room temperature[1]. The result is a lattice mismatch of 2.1% for $[110]_{EuO} \parallel [\bar{1}10]_{YAlO_3}$ and 1.3% for $[\bar{1}10]_{EuO} \parallel [001]_{YAlO_3}$ (ref. 6). The substrates were glued to a resistive heater using silver paint. The substrate heater was then installed in the deposition system, which was evacuated to its base pressure. The substrates were then heated in vacuum to their deposition temperature ($T_D \approx 580\,°C$). During substrate heating the chamber background pressure usually increased to about 5×10^{-6} mbar. Eu_2O_3 was deposited for 20 min by reactive radio-frequency magnetron sputtering at a power of $P_{rf} = 50$ W using an Ar/O_2 working gas mixture (total pressure $p_{tot} = 0.05$ mbar). To provide constant growth conditions during the deposition, both working gases were constantly renewed at flow rates of 2.0 sccm. After the Eu_2O_3 deposition, the films were capped with titanium by d.c. magnetron sputtering (deposition time = 4 min, $P_{d.c.} = 100$ W, argon working gas, $P_{tot} = 0.05$ mbar, argon flow = 4.0 sccm). Subsequently the heater was switched off and the films were cooled to room temperature in vacuum.

References

1. Eick, H. A., Baenziger, N. C. & Eyring, L. Lower oxides of samarium and europium. The preparation and crystal structure of $SmO_{0.4-0.6}$, SmO and EuO. *J. Am. Chem. Soc.* **78,** 5147–5149 (1956).
2. Rau, R. C. The crystal structure of Eu_3O_4. *Acta Crystallogr.* **20,** 716–723 (1966).
3. Yakel, H. L. A refinement of the crystal structure of monoclinic europium sesquioxide. *Acta Crystallogr. B* **35,** 564–569 (1979).
4. Bommer, H. Z. Die Gitterkonstanten der C-Formen der Oxyde der seltenen Erdmetalle. *Z. Anorg. Allg. Chem.* **241,** 273–280 (1939).
5. Matthias, B. T., Bozorth, R. M. & Van Vleck, J. H. Ferromagnetic interaction in EuO. *Phys. Rev. Lett.* **7,** 160–161 (1961).
6. Schmehl, A. *et al.* Epitaxial integration of the highly spin-polarized ferromagnetic semiconductor EuO with silicon and GaN. *Nat. Mater.* **6,** 882–887 (2007).
7. Swartz, A. G. *et al.* Epitaxial EuO thin films on GaAs. *Appl. Phys. Lett.* **97,** 112509 (2010).
8. Swartz, A. G., Odenthal, P. M., Hao, Y., Ruoff, R. S. & Kawakami, R. K. Integration of the ferromagnetic insulator EuO onto graphene. *ACS Nano* **6,** 10063 (2013).
9. Melville, A. *et al.* Epitaxial growth of europium monoxide on diamond. *Appl. Phys. Lett.* **103,** 22402 (2013).
10. Melville, A. *et al.* Lutetium-doped EuO films grown by molecular-beam epitaxy. *Appl. Phys. Lett.* **100,** 222101 (2012).
11. Shannon, R. D. & Rossi, R. C. Definition of topotaxy. *Nature* **202,** 1000–1001 (1964).
12. Mehl, R. F., McCandless, E. L. & Rhines, F. N. Orientation of oxide films on metals. *Nature* **134,** 1009 (1934).
13. Yamaguti, T. Oxidation of a crystal surface studied by means of cathode ray reflection. *Proc. Phys. Math. Soc. Jpn* **17,** 443–453 (1935).
14. Katz, G., Nicol, A. W. & Roy, R. New topotaxy in precipitation from spinel. *Nature* **223,** 609–610 (1969).
15. Rossi, R. C. & Fulrath, R. M. Epitaxial growth of spinel by reaction in the solid state. *J. Am. Ceram. Soc.* **46,** 145–149 (1963).
16. Tomioka, N. & Fujino, K. Natural $(Mg,Fe)SiO_3$-ilmenite and -perovskite in the Tenham Meteorite. *Science* **277,** 1084–1086 (1997).
17. Mehl, R. F. & McCandless, E. L. Orientation of oxide films on iron. *Nature* **137,** 702 (1936).
18. Cahn, R. W. Solid-state chemistry: topotaxy in metal-oxide reduction. *Nature* **316,** 297 (1985).
19. Revcolevschi, A. & Dhalenne, G. Crystallographically aligned metal-oxide composite made by reduction of a directionally solidified oxide-oxide eutectic. *Nature* **316,** 335–336 (1985).
20. Hayward, M. A., Green, M. A., Rosseinsky, M. J. & Sloan, J. Sodium hydride as a powerful reducing agent for topotactic oxide deintercalation: synthesis and characterization of the nickel(I) oxide $LaNiO_2$. *J. Am. Chem. Soc.* **121,** 8843–8854 (1999).
21. Tsujimoto, Y. *et al.* Infinite-layer iron oxide with a square-planar coordination. *Nature* **450,** 1062–1065 (2007).
22. Hadermann, J., Abakumov, A. M., Adkin, J. J. & Hayward, M. A. Topotactic reduction as a route to new close-packed anion deficient perovskites: structure and magnetism of $4H$-$BaMnO_{2+x}$. *J. Am. Chem. Soc.* **131,** 10598–10604 (2009).
23. Inoue, S. *et al.* Single-crystal epitaxial thin films of $SrFeO_2$ with FeO_2 'infinite layers'. *Appl. Phys. Lett.* **92,** 161911 (2008).
24. Kawai, M. *et al.* Reversible changes of epitaxial thin films from perovskite $LaNiO_3$ to infinite-layer structure $LaNiO_2$. *Appl. Phys. Lett.* **94,** 082102 (2009).
25. Inoue, S. *et al.* Anisotropic oxygen diffusion at low temperature in perovskite-structure iron oxides. *Nat. Chem.* **2,** 213–217 (2010).
26. Matsumoto, K. *et al.* Artificial superlattice thin film of infinite-layer structure $[CaFeO_2]/[SrFeO_2]$. *Appl. Phys. Express* **3,** 105601 (2010).
27. Zurbuchen, M. A. Topotactic anion exchange oxide films and method of producing the same. US Patent 7,208,044 B2 (2007).
28. Moon, E. J. *et al.* Fluorination of epitaxial oxides: synthesis of perovskite oxyfluoride thin films. *J. Am. Chem. Soc.* **136,** 2224–2227 (2014).
29. Pankratz, L. B. *Thermodynamic Properties of Elements and Oxides* (United States Bureau of Mines, 1982).
30. Ulbricht, R. W., Schmehl, A., Heeg, T., Schubert, J. & Schlom, D. G. Adsorption-controlled growth of EuO by molecular-beam epitaxy. *Appl. Phys. Lett.* **93,** 102105 (2008).
31. Sutarto, R. *et al.* Epitaxial and layer-by-layer growth of EuO thin films on yttria-stabilized cubic zirconia (001) using MBE distillation. *Phys. Rev. B* **79,** 205318 (2009).
32. Beukers, J. *et al.* Epitaxial EuO thin films by pulsed laser deposition monitored by *in situ* X-ray photoelectron spectroscopy. *Thin Solid Films* **518,** 5173–5176 (2010).
33. Yamasaki, T., Ueno, K., Tsukazaki, A., Fukumura, T. & Kawasaki, M. Observation of anomalous Hall effect in EuO epitaxial thin films grown by a pulse laser deposition. *Appl. Phys. Lett.* **98,** 082116 (2011).
34. Lee, K. & Suits, J. C. Reduction of ferromagnetic exchange with lattice dilation in EuO. *J. Appl. Phys.* **41,** 954–956 (1970).
35. Coburn, J. W. & Lee, K. Sputter deposition of EuO thin films. *J. Appl. Phys.* **42,** 5903–5905 (1971).
36. Barbagallo, M. *et al.* Experimental and theoretical analysis of magnetic moment enhancement in oxygen-deficient EuO. *Phys. Rev. B* **81,** 235216 (2010).
37. Barbagallo, M. *et al.* Thickness-dependent magnetic properties of oxygen-deficient EuO. *Phys. Rev. B* **84,** 075219 (2011).
38. Barin, I. & Platzki, G. *Thermochemical Data of Pure Substances* (VCH, 1995).
39. Kubinski, D. J., Hoffman, D. W. & Soltis, R. E. Reactive codeposition of *in situ* Y-Ba-Cu-O superconducting films using dilute mixtures of ozone in oxygen. *J. Appl. Phys.* **71,** 1860–1867 (1992).
40. Matijasevic, V. C. *et al.* MBE synthesis of $YBa_2Cu_3O_y$ superconducting thin films. *IEEE Trans. Appl. Supercond.* **3,** 1524–1527 (1993).
41. Appelboom, H. M. *et al.* Sm-Ba-Cu-O films grown at low temperature and pressure. *Physica C* **214,** 323–334 (1993).
42. Geller, S. & Wood, E. A. Crystallographic studies of perovskite-like compounds. I. Rare earth orthoferrites and $YFeO_3$, $YCrO_3$, $YAlO_3$. *Acta Crystallogr.* **9,** 563–568 (1965).
43. Oswald, H. R. Chemische Anwendungen der Elektronenmikroskopie: Topotaktische Reaktionen. *Angew. Chem.* **81,** 470 (1969).
44. Bailey, S. W. *et al.* Report of the International Mineralogical Association (IMA)—International Union of Crystallography (IUCr) Joint Committee of Nomenclature. *Acta Crystallogr. A* **33,** 681–684 (1977).
45. Mundy, J. A. *et al.* Hetero-epitaxial EuO interfaces studied by analytic electron microscopy. *Appl. Phys. Lett.* **104,** 091601 (2014).

46. Negusse, E. *et al.* Effect of electrode and EuO thickness on EuO-electrode interface in tunneling spin filter. *J. Appl. Phys.* **99,** 08E507 (2006).

47. Mairoser, T., Loder, F., Melville, A., Schlom, D. G. & Schmehl, A. Influence of chemical doping on the magnetic properties of EuO. *Phys. Rev. B* **87,** 014416 (2013).

48. McGuire, T. R. & Shafer, M. W. Ferromagnetic europium compounds. *J. Appl. Phys.* **35,** 984–988 (1964).

49. Mehl, R. F. & McCandless, E. L. Oxide films on iron. *Trans. Am. Inst. Mining Met. Eng.* **125,** 531–559 (1937).

50. Burgers, W. G. & van Amstel, J. J. A. P. 'Oriented' oxidation of barium. *Physica* **3,** 1057–1063 (1936).

Acknowledgements

Author contributions

T.M. grew the films, performed θ–2θ- and ϕ-scans and evaluated the orientation relationship in cooperation with A.S and D.G.S.; T.M. performed the superconducting quantum interference device measurements and evaluated the data; A.M. performed rocking scans and evaluated the data in cooperation with D.G.S.; J.A.M, D.H., P.C. and D.A.M. performed STEM and EELS measurement and interpreted the data; A.G. and J.S. performed X-ray reflectometry measurements and simulations; T.M., R.H. and D.G.S. did the thermodynamic calculations; A.S., D.G.S. and T.M. wrote the paper; all authors discussed the results and commented on the manuscript.

Additional information

Supplementary Information accompanies this paper at http://www.nature.com/naturecommunications.

Competing financial interests: The authors declare no competing financial interests.

Reprints and permission information is available online at http://npg.nature.com/reprintsandpermissions/

How to cite this article: Mairoser, T. *et al.* High-quality EuO thin films the easy way via topotactic transformation. *Nat. Commun.* 6:7716 doi: 10.1038/ncomms8716 (2015).